Computational study of the reaction between chloroacetone and OH radical

Nobuaki Tanaka*, Satoshi Yamagishi and Hiromasa Nishikiori

Department of Environmental Science and Technology, Faculty of Engineering, Shinshu University, 4-17-1 Wakasato, Nagano 380-8553, Japan

* Corresponding author. Tel.: +81 26 269 5527.

E-mail address: ntanaka@shinshu-u.ac.jp (N. Tanaka).

ABSTRACT

In this study, the reaction of the chloroacetone with OH radical was studied theoretically using density functional theory (DFT) and transition state theory. The potential energy surface of the reaction was calculated at the CAM-B3LYP/6-311++G(2d,2p) and M06-2X/6-311++G(2d,2p) levels. We initially considered four possible reaction paths: (1) the hydrogen atom abstraction from chloroacetone by OH radical; (2) the addition of the OH radical to the carbonyl carbon; (3) chlorine atom abstraction; and (4) S_N2 displacement. The conventional transition state theory was employed to calculate the rate constants. The hydrogen abstraction from the $–CH_2Cl$ group was found to be dominant. Since, the predicted total rate constant at the CAM-B3LYP/6-311++G(2d,2p) level was in good agreement with the experimental value at 298 K, the level of theory used in this study to describe this reaction is appropriate.

Keywords: chloroacetone; OH radical; DFT; OH addition; H-atom abstraction

1. Introduction

The OH radical plays a central role as an atmospheric oxidant. In the unpolluted troposphere, the OH radical is generated by the ozone photolysis-derived $O(^1D)$ reaction with water vapor, followed by the reaction with carbon monoxide or ozone to yield the hydroperoxy radical or with methane to yield the methylperoxy radical. Then, the hydroperoxy radical reacts with nitric oxide to reproduce the hydroxyl radical [1]. Additionally, in normal condition, the hydroxyl radical undergoes H-atom abstraction and/or addition reaction(s) with volatile organic compounds (VOCs). The VOC reaction leads to the formation of secondary organic aerosols (SOAs) [2], which affect the radiative balance [3].

Because of its important role in the upper troposphere and lower stratosphere [4], the OH radical reaction with acetone has been extensively studied both experimentally and theoretically [5, 6]. The abstraction product acetonyl radical is also an important intermediate species that yields peroxy radicals through the reaction with O_2 [7, 8]. From the environmental point of view strongly linked with the depletion of the ozone layer, Carr et al. investigated the gas-phase reaction of the OH radical with halogenated acetones and determined the rate constants at 298 K [9]. However, since the product analysis has not been carried out yet, the detailed mechanism of chloroacetone oxidation remains uncertain. Computational studies can be useful for evaluating the possible mechanism of the oxidation. In this paper, we present the analysis of the reaction of the chloroacetone with the OH radical obtained by density functional theory (DFT) calculations. We consider the following possible reaction paths.

$$CH_2ClCOCH_3 + OH \rightarrow CHClCOCH_3 + H_2O \quad (1a)$$

$$CH_2ClCOCH_3 + OH \rightarrow CH_2ClCOCH_2 + H_2O \quad (1b)$$

$CH_2ClCOCH_3 + OH \rightarrow CH_2ClCO(OH)CH_3$ (2)

$CH_2ClCOCH_3 + OH \rightarrow CH_2COCH_3 + HOCl$ (3)

$CH_2ClCOCH_3 + OH \rightarrow CH_2(OH)COCH_3 + Cl$ (4)

2. Computational methods

The equilibrium geometries of the reactants, transition states, products and complexes were optimized using the DFT method. Range-separated hybrid generalized gradient approximation (GGA) functional CAM-B3LYP [10] and hybrid meta-GGA functional M06-2X [11] were employed using the 6-311++G(2d,2p) basis set. The harmonic vibrational frequencies were calculated to confirm the predicted structures as local minima or transition states (one imaginary frequency) and to elucidate the zero-point vibrational energy (ZPE) corrections. The obtained transition states were confirmed as those connecting the investigational species by a calculation of the subsequent intrinsic reaction coordinates. All the calculations were performed using Gaussian 09 [12]. The spin-squared values were checked and the deviations from the doublet value of $<s^2> = 0.75$ were found to be lower than 3.9%. Therefore, the spin contamination was negligible for all the studied radical species.

The rate constants for the addition and abstraction reactions were estimated using the conventional thermodynamic formulation of transition state theory. The rate constant k is given by

$$k(T) = \kappa \frac{k_B T}{h} e^{-\Delta G^{\neq}/RT} \quad (5)$$

where k_B is the Boltzmann constant, T is the temperature, h is Planck's constant, $\Delta G^{\neq}$ is the Gibbs free energy of activation and κ is the transmission coefficient. The tunneling effect was approximated using the Wigner correction [13]. In case the abstraction

reaction proceeds via complex formation the rate constant k is given by

$$k(T) = \left(\frac{k_a}{k_{-a}}\right) k_b = K_{\mathrm{eq}} k_b \qquad (6)$$

where k_a and k_{-a} are the rate constants for the formation and dissociation of the complex, respectively, and k_b corresponds to the consecutive abstraction reaction [14].

3. Results and discussion

Four types of reaction paths have been investigated for the OH + $CH_2ClCOCH_3$ reaction, namely (1) hydrogen atom abstraction, (2) OH addition, (3) chlorine atom abstraction and (4) S_N2 displacement. In the gas phase, chloroacetone in the gauche form exists as a stable conformer by 299 cm^{-1} compared with that in the syn form [15]. Therefore, both gauche and syn forms were considered as reactants. The optimized structures of reactants, products, complexes and transition states are shown in Fig. 1. The selected bond lengths calculated at the (U)CAM-B3LYP/6-311++G(2d,2p) level of theory are listed in Table 1. The energies and harmonic vibrational frequencies for the reactants, complexes, transition states and addition products are summarized in Tables S1 and S2, respectively. Table 2 lists the relative electronic energies, including the zero-point vibrational energies ($\Delta_r E$), relative enthalpies at 298 K ($\Delta_r H$) and relative Gibbs energies at 298 K ($\Delta_r G$) of the addition products and complexes to the isolated reactants. Because of the high activation energies, the contribution of the chlorine atom abstraction ($\Delta G^{\neq}$ = 33.0 and 32.7 kcal mol^{-1} for $TS_{Cl\text{-}abs\ 1}$ and $TS_{Cl\text{-}abs\ 3}$, respectively) and S_N2 displacement ($\Delta G^{\neq}$ = 48.3 and 34.2 kcal mol^{-1} for $TS_{gauche\ SN2}$ and $TS_{syn\ SN2}$, respectively) should be negligible. Therefore, we will focus on the hydrogen abstraction and OH addition reactions. Fig. 2 represents the schematic Gibbs energy profiles of the relevant reaction pathways.

3.1.1. Hydrogen atom abstraction

Table 3 lists the $\Delta E^{\neq}$, $\Delta H^{\neq}$ and $\Delta G^{\neq}$ values for the H-atom abstraction reactions. The hydrogen abstraction reaction proceeds via two transition states for *gauche*-chloroacetone, $TS_{abs\ gauche\ C1}$ and $TS_{abs\ gauche\ C3}$, via other two transition states for *syn*-chloroacetone, $TS_{abs\ syn\ C1}$ and $TS_{abs\ syn\ C3}$. In $TS_{abs\ gauche\ C1}$ and $TS_{abs\ syn\ C1}$, the OH radical abstracts the hydrogen atom from the $–CH_2Cl$ group, while in $TS_{abs\ gauche\ C3}$ and $TS_{abs\ syn\ C3}$ from the $–CH_3$ group. (Intrinsic reaction coordinate IRC) calculations revealed that $TS_{abs\ gauche\ C1}$ is connected with the $complex_{gauche\ 1}$. As shown in Table 3, the breaking C–H bond are elongated on average by 8.5% compared with the equilibrium C–H bond length of chloroacetone, while the forming O–H bonds are elongated on average by 44% compared with the O–H bond of H_2O at equilibrium. The reactant-like geometry is characteristic of an early transition state. The $\Delta G^{\neq}$ values obtained using the UM06-2X functional are larger than those obtained using the UCAM-B3LYP functional in the range of 1.6 ($TS_{abs\ gauche\ C1}$) to 2.3 ($TS_{abs\ gauche\ C3}$) kcal mol^{-1}. The $\Delta G^{\neq}$ values of $TS_{abs\ gauche\ C1}$ and $TS_{abs\ syn\ C1}$ are relatively smaller than those of $TS_{abs\ gauche\ C3}$ and $TS_{abs\ syn\ C3}$, respectively, mainly because of the differences in the C–H bond strength. At the (U)CAM-B3LYP/6-311++G(2d,2p) level, the difference in the C–H bond dissociation enthalpy in the $–CH_2Cl$ group from that of the $–CH_3$ group was calculated to be −6.3 and −7.2 kcal mol^{-1} for the *gauche*- and *syn*-conformers, respectively. The Cl substitution lowered the bond strength of the C–H bond of the $–CH_2Cl$ group [9]. The rate constants for the H-atom abstraction from the $–CH_2Cl$ group were calculated to be one order of magnitude larger than those from the $–CH_3$ group.

3.1.2. OH addition

The OH radical can attach to the carbon atom of the carbonyl group to form the OH adduct of chloroacetone. Depending on the different conformations of chloroacetone and the relative direction of the O–H bond to the carbonyl group of chloroacetone, four stationary points (i.e. $add_{gauche\ 1}$, $add_{gauche\ 1\_2}$, $add_{gauche\ 2}$ and add_{syn}) were identified. In $add_{gauche\ 1\_2}$ and add_{syn}, the O–H bond points towards the Cl atom. The O–H stretching vibrational frequencies of $add_{gauche\ 1\_2}$ and add_{syn} were red-shifted by 20 and 24 cm^{-1}, respectively, from that of $add_{gauche1}$ (Table S2), probably because of the presence of weak intramolecular hydrogen bonds. The second-order perturbation analysis of the natural bond orbital (NBO) Fock matrix [16] gave $n_{Cl} \rightarrow \sigma^*_{OH}$ interactions of 0.60 and 0.31 kcal mol^{-1} in magnitude for $add_{gauche\ 1\_2}$ and add_{syn}, respectively, while the interactions for $add_{gauche\ 1}$ and $add_{gauche\ 2}$ were smaller than 0.25 kcal mol^{-1}. The transition states $TS_{add\ gauche\ 1}$, $TS_{add\ gauche\ 2}$ and $TS_{add\ syn}$ correspond to the formation of the addition products, $add_{gauche\ 1}$, $add_{gauche\ 2}$ and add_{syn} respectively. The imaginary frequencies and relative energies of the transition states and distance ratios of $r_{C\cdots OH}/r_{C–OH}$ are summarized in Table 4. The C⋯OH distances in the transition states are elongated by over 34% compared with those of the addition products, indicating an early transition state. In contrast to the H-atom abstraction reaction, the $\Delta G^{\neq}$ values for the addition reaction calculated with the two methods differ by less than 0.4 kcal mol^{-1}. The $\Delta G^{\neq}$ value for the addition of OH to *syn*-chloroacetone is found to be slightly smaller than that to *gauche*-chloroacetone. The barrier heights for the OH addition reaction are calculated to be higher than those for the H-atom abstraction reaction. A similar reactivity trend has been reported for acetone and fluoroacetone.

By taking the symmetry factor and Boltzmann ratio into consideration, with the

CAM-B3LYP or M06-2X method, the total rate constant was calculated to be 3.24 × 10^{-13} or 2.78 × 10^{-14} cm^3 $molecule^{-1}$ s^{-1} at 298 K, respectively. The hydrogen abstraction from the $–CH_2Cl$ group was found to be dominant. The CAM-B3LYP value is in good agreement with the experimentally obtained value of (4.2 ± 0.8) × 10^{-13} cm^3 $molecule^{-1}$ s^{-1} [9]. The total rate constants calculated at the CAM-B3LYP/6-311++G(2d,2p) level over the temperature range 200–360 K are plotted in the Arrhenius form in Fig. 3. The two-parameter Arrhenius equation is

$$k_{total}(T) = 5.82 \times 10^{-15} \exp(1207/T)\ cm^3\ molecule^{-1}\ s^{-1}.$$

The Arrhenius plot of k_{total} shows a slight deviation from linearity. Similar deviations were observed for the acetone + OH [5] and hydroxyacetone + OH [17] reactions. The three-parameter equation is

$$k_{total}(T) = 1.02 \times 10^{-22}\, T^{2.7} \exp(1924/T)\ cm^3\ molecule^{-1}\ s^{-1}.$$

Conclusions

The reaction between the chloroacetone and OH radical has been studied theoretically using density functional theory and transition state theory. The potential energy surface of the reaction was calculated at the CAM-B3LYP/6-311++G(2d,2p) and M06-2X/6-311++G(2d,2p) levels, with which we analyzed two important reaction paths: (1) the hydrogen atom abstraction from chloroacetone by OH radical; and (2) the addition of the OH radical to the carbonyl carbon. The conventional transition state theory was employed to calculate the rate constants. The hydrogen abstraction from the $–CH_2Cl$ group was found to be dominant. The predicted total rate constant at the CAM-B3LYP/6-311++G(2d,2p) level is in good agreement with the experimental value at 298 K. The temperature dependence of the total rate constant was fitted by the

expression $k_{total}(T) = 1.02 \times 10^{-22} T^{2.7} \exp(1924/T)$ cm^3 molecule^{-1} s^{-1}.

References

[1] H. Levy II, Normal atomosphere: Large radical and formaldehyde concentrations predicted, Science, 173 (1971) 141.

[2] M. Kanakidou, J.H. Seinfeld, S.N. Pandis, I. Barnes, F.J. Dentener, M.C. Facchini, R. Van Dingenen, B. Ervens, A. Nenes, C.J. Nielsen, E. Swietlicki, J.P. Putaud, Y. Balkanski, S. Fuzzi, J. Horth, G.K. Moortgat, R. Winterhalter, C.E.L. Myhre, K. Tsigaridis, E. Vignati, E.G. Stephanou, J. Wilson, Organic aerosol and global climate modelling: a review, Atmos Chem Phys, 5 (2005) 1053-1123.

[3] P. Forster, V. Ramaswamy, P. Artaxo, T. Berntsen, R. Betts, D.W. Fahey, J. Haywood, J. Lean, D.C. Lowe, G. Myhre, J. Nganga, R. Prinn, G. Raga, M. Schulz, R.V. Dorland, Changes in Atmospheric Constituents and in Radiative Forcing, in: S. Solomon, D. Qin, M. Manning, Z. Chen, M. Marquis, K.B. Averyt, M.Tignor, H.L. Miller (Eds.) Climate Change 2007: The Physical Science Basis. Contribution of Working Group I to the Fourth Assessment Report of the Intergovernmental Panel on Climate Change, Cambridge University Press, Cambridge, United Kingdom and New York, NY, USA, 2007.

[4] H.B. Singh, M. Kanakidou, P.J. Crutzen, D.J. Jacob, High-concentrations and photochemical fate of oxygenated hydrocarbons in the global troposphere, Nature, 378 (1995) 50-54.

[5] T. Yamada, P.H. Taylor, A. Goumri, P. Marshall, The reaction of OH with acetone and acetone-d(6) from 298 to 832 K: Rate coefficients and mechanism, J Chem Phys, 119 (2003) 10600-10606.

[6] M. Wollenhaupt, S.A. Carl, A. Horowitz, J.N. Crowley, Rate coefficients for reaction of OH with acetone between 202 and 395 K, J Phys Chem A, 104 (2000) 2695-2705.

[7] K. Imrik, E. Farkas, G. Vasvari, I. Szilagyi, D. Sarzynski, S. Dobe, T. Berces, F. Marta, Laser spectrometry and kinetics of selected elementary reactions of the acetonyl radical, Phys Chem Chem Phys, 6 (2004) 3958-3968.

[8] M. Hassouna, E. Delbos, P. Devolder, B. Viskolcz, C. Fittschen, Rate and equilibrium constant of the reaction of 1-methylvinoxy radicals with O_2: $CH_3COCH_2+O_2 \rightarrow CH_3COCH_2O_2$, J Phys Chem A, 110 (2006) 6667-6672.

[9] S. Carr, D.E. Shallcross, C. Canosa-Mas, J.C. Wenger, H.W. Sidebottom, J.J. Treacy, R.P. Wayne, A kinetic and mechanistic study of the gas-phase reactions of OH radicals and Cl atoms with some halogenated acetones and their atmospheric implications, Phys

Chem Chem Phys, 5 (2003) 3874-3883.
[10] T. Yanai, D.P. Tew, N.C. Handy, A new hybrid exchange-correlation functional using the Coulomb-attenuating method (CAM-B3LYP), Chem Phys Lett, 393 (2004) 51-57.
[11] D.G. Truhlar, Y. Zhao, The M06 suite of density functionals for main group thermochemistry, thermochemical kinetics, noncovalent interactions, excited states, and transition elements: two new functionals and systematic testing of four M06-class functionals and 12 other functionals, Theor Chem Acc, 120 (2008) 215-241.
[12] M.J. Frisch, G.W. Trucks, H.B. Schlegel, G.E. Scuseria, M.A. Robb, J.R. Cheeseman, G. Scalmani, V. Barone, B. Mennucci, G.A. Petersson, H. Nakatsuji, M. Caricato, X. Li, H.P. Hratchian, A.F. Izmaylov, J. Bloino, G. Zheng, J.L. Sonnenberg, M. Hada, M. Ehara, K. Toyota, R. Fukuda, J. Hasegawa, M. Ishida, T. Nakajima, Y. Honda, O. Kitao, H. Nakai, T. Vreven, J. Montgomery, J. A., J.E. Peralta, F. Ogliaro, M. Bearpark, J.J. Heyd, E. Brothers, K.N. Kudin, V.N. Staroverov, R. Kobayashi, J. Normand, K. Raghavachari, A. Rendell, J.C. Burant, S.S. Iyengar, J. Tomasi, M. Cossi, N. Rega, N.J. Millam, M. Klene, J.E. Knox, J.B. Cross, V. Bakken, C. Adamo, J. Jaramillo, R. Gomperts, R.E. Stratmann, O. Yazyev, A.J. Austin, R. Cammi, C. Pomelli, J.W. Ochterski, R.L. Martin, K. Morokuma, V.G. Zakrzewski, G.A. Voth, P. Salvador, J.J. Dannenberg, S. Dapprich, A.D. Daniels, Ö. Farkas, J.B. Foresman, J.V. Ortiz, J. Cioslowski, D.J. Fox, Gaussian 09, Revision B.01, Gaussian, Inc., Wallingford, 2010.
[13] E. Wigner, Crossing of potential thresholds in chemical reactions, Z Phys Chem, B19 (1932) 203-216.
[14] D.L. Singleton, R.J. Cvetanovic, Temperature dependence of the reactions of oxygen atoms with olefins, J Am Chem Soc, 98 (1976) 6812-6819.
[15] C.T. Au, Y.Q. Zhang, C.F. Ng, H.L. Wan, Oxidative coupling of methane over LaF_3/La_2O_3 catalysts, Catal Lett, 23 (1994) 377-386.
[16] A.E. Reed, L.A. Curtiss, F. Weinhold, Intermolecular interaction from a natural bond orbital, donor-acceptor viewpoint, Chem Rev, 88 (1988) 899-926.
[17] A. Galano, Theoretical study on the reaction of tropospheric interest: Hydroxyacetone plus OH. Mechanism and kinetics, J Phys Chem A, 110 (2006) 9153-9160.

Figure captions

Fig. 1. Optimized structures of the reactants, complexes, OH addition products, transition states and abstraction products calculated at the

(U)CAM-B3LYP/6-311++G(2d,2p) level of theory.

Fig. 2. Schematic Gibbs energy profiles for the OH addition and H-atom abstraction reactions of chloroacetone + OH calculated at the (U)CAM-B3LYP/6-311++G(2d,2p) level of theory.

Fig. 3. Arrhenius plot of the total rate constant in the temperature range 200–360 K. Solid line: two-parameter fitting. Dashed line: three-parameter fitting.

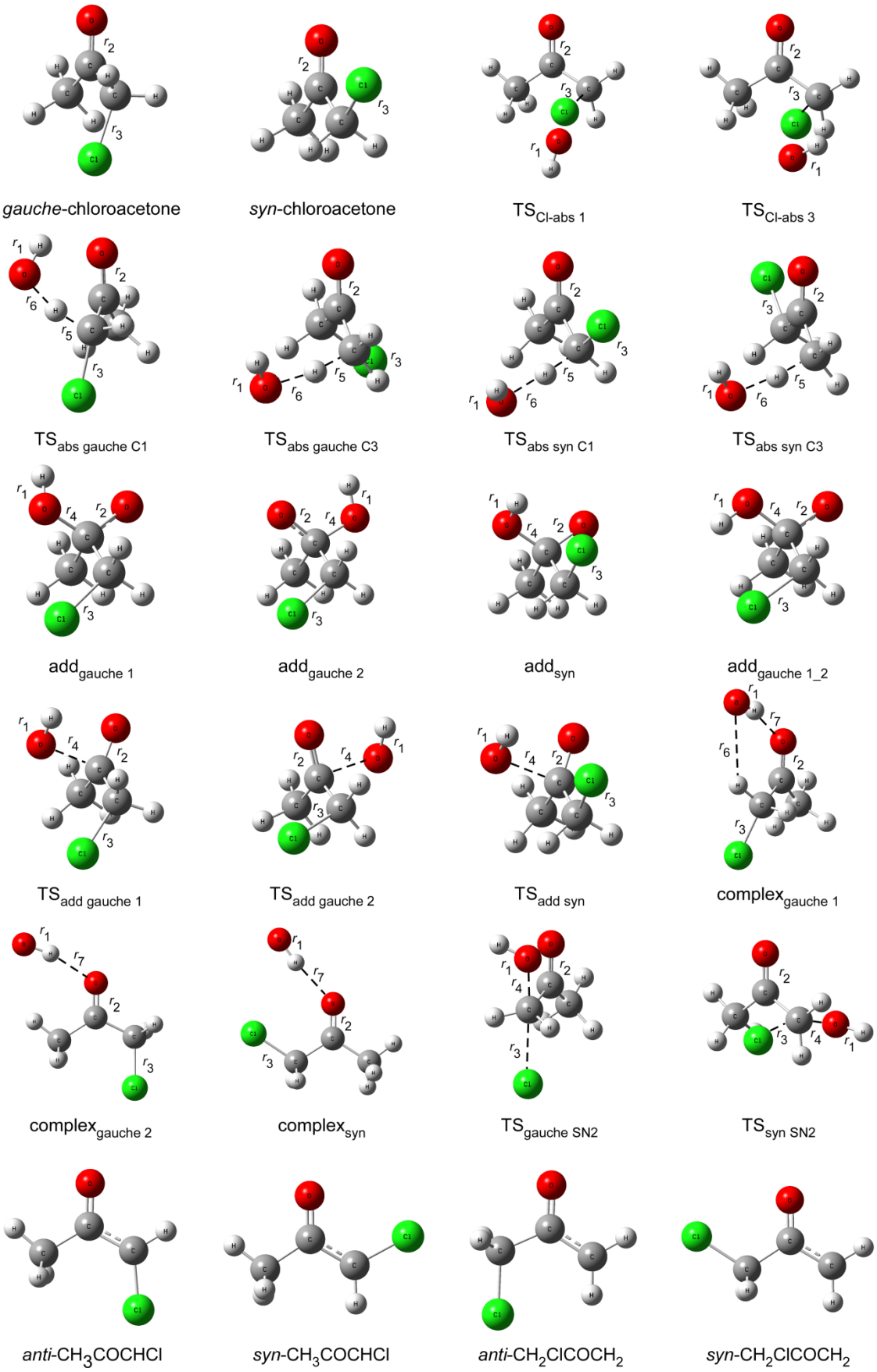
gauche-chloroacetone
syn-chloroacetone
$TS_{Cl\text{-}abs\ 1}$
$TS_{Cl\text{-}abs\ 3}$
$TS_{abs\ gauche\ C1}$
$TS_{abs\ gauche\ C3}$
$TS_{abs\ syn\ C1}$
$TS_{abs\ syn\ C3}$
$add_{gauche\ 1}$
$add_{gauche\ 2}$
add_{syn}
$add_{gauche\ 1\_2}$
$TS_{add\ gauche\ 1}$
$TS_{add\ gauche\ 2}$
$TS_{add\ syn}$
$complex_{gauche\ 1}$
$complex_{gauche\ 2}$
$complex_{syn}$
$TS_{gauche\ SN2}$
$TS_{syn\ SN2}$
anti-$CH_3COCHCl$
syn-$CH_3COCHCl$
anti-$CH_2ClCOCH_2$
syn-$CH_2ClCOCH_2$

Fig. 1

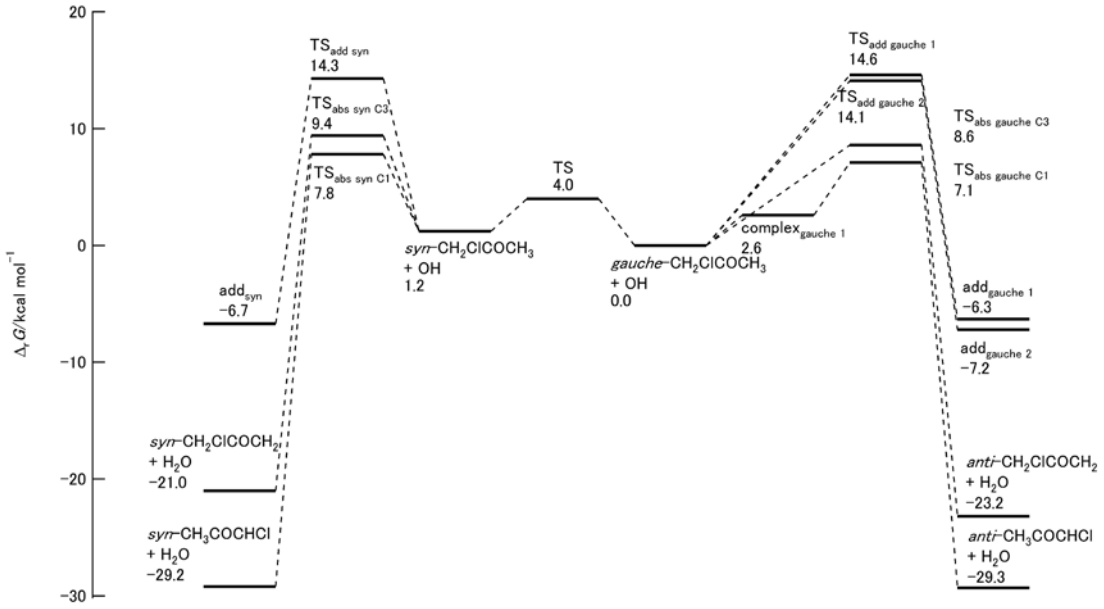
20
10
0
−10
−20
−30
$\Delta_r G$/kcal mol^{-1}
$TS_{add\ syn}$
14.3
$TS_{abs\ syn\ C3}$
9.4
$TS_{abs\ syn\ C1}$
7.8
TS
4.0
$TS_{add\ gauche\ 1}$
14.6
$TS_{add\ gauche\ 2}$
14.1
$TS_{abs\ gauche\ C3}$
8.6
$TS_{abs\ gauche\ C1}$
7.1
add_{syn}
−6.7
syn-$CH_2ClCOCH_3$
+ OH
1.2
gauche-$CH_2ClCOCH_3$
+ OH
0.0
$complex_{gauche\ 1}$
2.6
$add_{gauche\ 1}$
−6.3
$add_{gauche\ 2}$
−7.2
syn-$CH_2ClCOCH_2$
+ H_2O
−21.0
anti-$CH_2ClCOCH_2$
+ H_2O
−23.2
syn-$CH_3COCHCl$
+ H_2O
−29.2
anti-$CH_3COCHCl$
+ H_2O
−29.3

Fig. 2

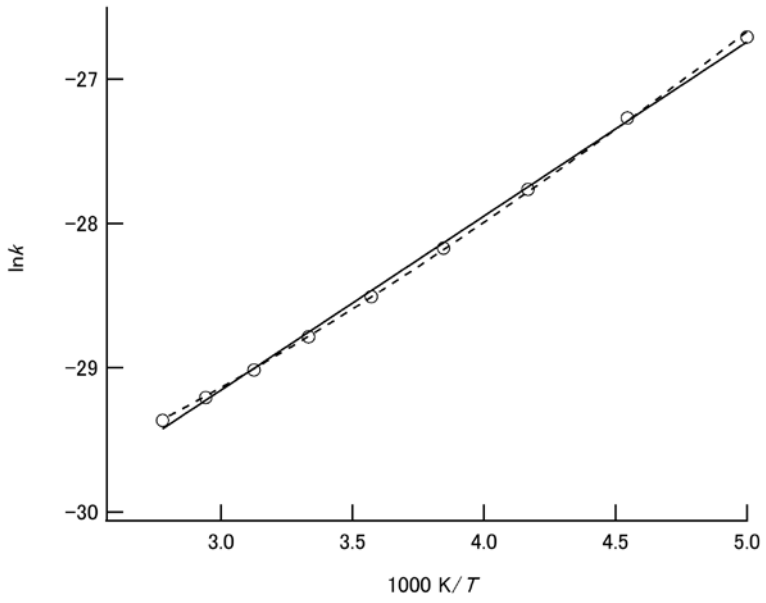
−27
−28
−29
−30
ln*k*
3.0
3.5
4.0
4.5
5.0
1000 K/*T*

Fig. 3

Table 1

Selected geometrical parameters (Å) optimized at the (U)CAM-B3LYP/6-311++G(2d,2p) level[a].

species	r_1	r_2	r_3	r_4	r_5	r_6	r_7
gauche-chloroacetone		1.204	1.792				
syn-chloroacetone		1.198	1.774				
OH	0.971						
H_2O	0.959						
$TS_{abs\ gauche\ C1}$	0.972	1.207	1.761		1.196	1.330	
$TS_{abs\ gauche\ C3}$	0.970	1.205	1.796		1.186	1.374	
$TS_{abs\ syn\ C1}$	0.971	1.199	1.753		1.159	1.436	
$TS_{abs\ syn\ C3}$	0.970	1.200	1.773		1.187	1.365	
$add_{gauche\ 1}$	0.961	1.343	1.786	1.405			
$add_{gauche\ 1\_2}$	0.962	1.338	1.795	1.405			
$add_{gauche\ 2}$	0.961	1.334	1.782	1.419			
add_{syn}	0.963	1.353	1.795	1.402			
$TS_{add\ gauche\ 1}$	0.971	1.247	1.787	1.915			
$TS_{add\ gauche\ 2}$	0.971	1.247	1.800	1.916			
$TS_{add\ syn}$	0.972	1.239	1.781	1.921			
$TS_{Cl\text{-}abs\ 1}$	0.965	1.215	2.265				
$TS_{Cl\text{-}abs\ 3}$	0.966	1.216	2.264				
$TS_{gauche\ SN2}$	0.969	1.231	2.429	1.771			
$TS_{syn\ SN2}$	0.968	1.199	2.138	1.845			
$complex_{gauche\ 1}$	0.983	1.211	1.789			2.664	1.873
$complex_{gauche\ 2}$	0.982	1.210	1.788				1.876
$complex_{syn}$	0.979	1.203	1.773				1.931

[a] Geometrical parameters are shown in Fig. 1.

Table 2

Thermochemical parameters (kcal mol^{-1}) of products.

stationary point	functional	$\Delta_r E$	$\Delta_r H$	$\Delta_r G$
$add_{gauche\ 1}$	UCAM-B3LYP	−16.2	−17.5	−6.3
	UM06-2X	−18.4	−19.8	−8.5
$add_{gauche\ 1\_2}$	UCAM-B3LYP	−15.8	−17.3	−5.6
	UM06-2X	−18.5	−19.9	−8.5
$add_{gauche\ 2}$	UCAM-B3LYP	−17.0	−18.2	−7.2
	UM06-2X	−19.0	−20.3	−9.2
add_{syn}	UCAM-B3LYP	−16.8	−18.2	−6.7
	UM06-2X	−19.4	−20.9	−9.5
$complex_{gauche\ 1}$	UCAM-B3LYP	−4.9	−5.3	2.6
	UM06-2X	−4.9	−5.3	2.5
$complex_{gauche\ 2}$	UCAM-B3LYP	−4.6	−5.0	2.2
	UM06-2X	−4.8	−5.3	2.5
$complex_{syn}$	UCAM-B3LYP	−3.8	−4.0	3.3

Table 3

Calculated imaginary frequencies, ratios of HO and CH distances, and thermochemical parameters (kcal mol^{-1}) of the transition states and rate constants for abstraction reactions.

stationary point	functional	ν/cm^{-1}	$r_{H\cdots OH}/\ r_{H-OH}$	$r_{C\cdots H}/\ r_{C-H}$	$\Delta E^{\neq}$	$\Delta H^{\neq}$	$\Delta G^{\neq}$	k/cm^3 $molecule^{-1}$ s^{-1}
$TS_{abs\ gauche\ C1}$	UCAM-B3LYP	1112i	1.39	1.10	−1.7	−2.6	7.1	1.46×10^{-13}
	UM06-2X	1378i	1.40	1.10	0.1	−0.8	8.7	1.26×10^{-14}
$TS_{abs\ gauche\ C3}$	UCAM-B3LYP	784i	1.43	1.09	0.7	0.0	8.6	8.08×10^{-15}
	UM06-2X	1133i	1.45	1.08	3.1	2.3	10.9	2.18×10^{-16}
$TS_{abs\ syn\ C1}$	UCAM-B3LYP	462i	1.50	1.07	−1.4	−2.0	6.6	1.79×10^{-13}
	UM06-2X	989i	1.48	1.07	0.3	−0.4	8.3	1.76×10^{-14}
$TS_{abs\ syn\ C3}$	UCAM-B3LYP	815i	1.42	1.09	0.1	−0.7	8.2	1.67×10^{-14}
	UM06-2X	1151i	1.44	1.08	2.2	1.3	10.2	7.91×10^{-16}

Table 4

Calculated imaginary frequencies, CO distance ratios and thermochemical parameters (kcal mol^{-1}) of the transition states and rate constants for addition reactions.

stationary point	functional	ν/cm^{-1}	$r_{C\cdots OH}$/ r_{C-OH}	$\Delta E^{\neq}$	$\Delta H^{\neq}$	$\Delta G^{\neq}$	k/cm^3 $molecule^{-1}$ s^{-1}
$TS_{add\ gauche\ 1}$	UCAM-B3LYP	458i	1.36	4.9	3.7	14.6	2.29×10^{-19}
	UM06-2X	614i	1.35	5.6	4.5	15.0	1.54×10^{-19}
$TS_{add\ gauche\ 2}$	UCAM-B3LYP	454i	1.35	4.4	3.3	14.1	6.19×10^{-19}
	UM06-2X	622i	1.34	5.2	4.1	14.4	3.62×10^{-19}
$TS_{add\ syn}$	UCAM-B3LYP	460i	1.30	3.3	2.0	13.2	2.78×10^{-18}
	UM06-2X	627i	1.35	3.9	2.5	13.6	1.63×10^{-18}

Table S1

Zero-point corrected energies (Hartree) of the reactants, complexes, OH addition products, transition states and abstraction products calculated at the (U)CAM-B3LYP/6-311++G(2d,2p) level.

species	energies
gauche-chloroacetone	−652.671403
syn-chloroacetone	−652.669505
OH	−75.729766
H_2O	−76.412417
$TS_{abs\ gauche\ C1}$	−728.403822
$TS_{abs\ gauche\ C3}$	−728.399987
$TS_{abs\ syn\ C1}$	−728.401438
$TS_{abs\ syn\ C3}$	−728.399034
$add_{gauche\ 1}$	−728.427044
$add_{gauche\ 1\_2}$	−728.426395
$add_{gauche\ 2}$	−728.428244
add_{syn}	−728.427978
$TS_{add\ gauche\ 1}$	−728.393355
$TS_{add\ gauche\ 2}$	−728.394103
$TS_{add\ syn}$	−728.394016
$TS_{Cl\text{-}abs\ 1}$	−728.360957
$TS_{Cl\text{-}abs\ 3}$	−728.361451
$TS_{gauche\ SN2}$	−728.339822
$TS_{syn\ SN2}$	−728.360809
$complex_{gauche\ 1}$	−728.408952
$complex_{gauche\ 2}$	−728.408507
$complex_{syn}$	−728.407154
anti-$CH_3COCHCl$	−652.035505
syn-$CH_3COCHCl$	−652.033714
anti-$CH_2ClCOCH_2$	−652.025351
syn-$CH_2ClCOCH_2$	−652.021976

Table S2

Harmonic vibrational frequencies of the stationary points calculated at the (U)CAM-B3LYP/6-311++G(2d,2p) level.

species	frequencies/cm^{-1}
gauche-chloroacetone	23, 169, 221, 405, 473, 518, 745, 830, 1013, 1056, 1209, 1265, 1299, 1413, 1458, 1473, 1483, 1822, 3075, 3116, 3133, 3182, 3188
syn-chloroacetone	35, 98, 212, 355, 467, 583, 781, 828, 856, 978, 1057, 1193, 1222, 1340, 1408, 1458, 1478, 1490, 1849, 3066, 3101, 3124, 3149, 3177
OH	3756
H_2O	1634, 3861, 3962
$TS_{abs\ gauche\ C1}$	1112i, 30, 120, 168, 223, 385, 409, 479, 529, 556, 757, 812, 887, 922, 1012, 1071, 1241, 1277, 1282, 1411, 1472, 1480, 1512, 1798, 3075, 3134, 3154, 3184, 3741
$TS_{abs\ gauche\ C3}$	784i, 24, 63, 76, 166, 208, 335, 399, 500, 549, 749, 817, 841, 855, 979, 1031, 1156, 1206, 1267, 1297, 1316, 1369, 1467, 1479, 1807, 3118, 3129, 3202, 3212, 3780
$TS_{abs\ syn\ C1}$	462i, 40, 66, 102, 126, 145, 214, 357, 480, 583, 698, 790, 837, 875, 983, 1072, 1186, 1191, 1312, 1340, 1410, 1480, 1564, 1839, 3068, 3128, 3140, 3179, 3771
$TS_{abs\ syn\ C3}$	815i, 35, 48, 96, 163, 211, 327, 377, 475, 579, 779, 788, 857, 867, 966, 992, 1105, 1197, 1224, 1287, 1350, 1371, 1458, 1465, 1829, 3100, 3113, 3150, 3202, 3780
$add_{gauche\ 1}$	99, 144, 202, 229, 307, 343, 433, 475, 559, 744, 805, 888, 923, 968, 1043, 1082, 1174, 1274, 1307, 1340, 1394, 1476, 1483, 1500, 3087, 3139, 3172, 3181, 3208, 3865
$add_{gauche\ 1\_2}$	114, 202, 225, 274, 3324, 337, 432, 476, 566, 740, 793, 886, 943, 959, 1045, 1102, 1182, 1258, 1293, 1320, 1400, 1477, 1484, 1502, 3085, 3141, 3166, 3182, 3212, 3845
$add_{gauche\ 2}$	92, 129, 202, 219, 319, 338, 396, 447, 557, 754, 812, 893, 929, 957, 1046, 1100, 1160, 1213, 1311, 1318, 1403, 1477, 1486, 1502, 3089, 3136, 3168, 3196, 3202, 3866

add_{syn}	104, 184, 198, 270, 320, 331, 436, 497, 543, 763, 817, 889, 922, 955, 1026, 1118, 1181, 1274, 1301, 1346, 1404, 1471, 1485, 1504, 3088, 3135, 3180, 3207, 3841
$TS_{add\ gauche\ 1}$	458i, 77, 163, 200, 247, 261, 295, 427, 450, 500, 758, 823, 838, 866, 1017, 1033, 1192, 1273, 1309, 1416, 1465, 1469, 1488, 1564, 3074, 3113, 3156, 3195, 3196, 3765
$TS_{add\ gauche\ 2}$	454i, 79, 169, 172, 215, 238, 295, 388, 482, 536, 737, 818, 835, 916, 1013, 1042, 1168, 1269, 1307, 1416, 1471, 1478, 1492, 1562, 3084, 3144, 3152, 3187, 3216, 3766
$TS_{add\ syn}$	460i, 96, 152, 186, 238, 284, 354, 366, 451, 566, 773, 833, 856, 884, 983, 1036, 1200, 1207, 1344, 1412, 1463, 1472, 1492, 1587, 3074, 3109, 3144, 3181, 3185, 3754
$TS_{Cl\text{-}abs\ 1}$	421i, 46, 68, 88, 94, 140, 158, 377, 429, 525, 564, 690, 825, 910, 926, 1057, 1086, 1121, 1268, 1412, 1467, 1484, 1489, 1713, 3069, 3129, 3174, 3179, 3284, 3826
$TS_{Cl\text{-}abs\ 3}$	421i, 36, 74, 93, 96, 145, 177, 378, 431, 526, 567, 688, 826, 912, 926, 1058, 1086, 1126, 1268, 1414, 1467, 1484, 1489, 1711, 3069, 3129, 3175, 3179, 3285, 3822
$TS_{gauche\ SN2}$	619i, 72, 201, 219, 253, 264, 387, 461, 491, 573, 611, 820, 834, 868, 1007, 1043, 1101, 1107, 1298, 1395, 1411, 1438, 1446, 1668, 3075, 3136, 3180, 3230, 3344, 3787
$TS_{syn\ SN2}$	981i, 91, 118, 131, 158, 180, 194, 303, 394, 532, 584, 796, 869, 897, 1060, 1064, 1073, 1136, 1253, 1405, 1416, 1484, 1487, 1838, 3068, 3076, 3140, 3183, 3281, 3796
$complex_{gauche\ 1}$	41, 43, 63, 163, 175, 226, 405, 441, 483, 532, 624, 751, 836, 850, 1017, 1057, 1214, 1279, 1314, 1415, 1456, 1470, 1482, 1796, 3076, 3108, 3134, 3179, 3185, 3554
$complex_{gauche\ 2}$	19, 33, 39, 163, 167, 227, 421, 468, 481, 527, 593, 751, 829, 851, 1016, 1057, 1216, 1275, 1304, 1418, 1455, 1473, 1483, 1801, 3075, 3117, 3134, 3178, 3184, 3571
$complex_{syn}$	27, 46, 56, 101, 145, 221, 362, 426, 467, 530, 591, 787, 827, 862, 989, 1057, 1200, 1226, 1346, 1412, 1455,

	1477, 1490, 1834, 3068, 3101, 3128, 3149, 3180, 3635
anti-$CH_3COCHCl$	122, 151, 214, 451, 491, 503, 661, 788, 941, 1013, 1044, 1263, 1338, 1418, 1479, 1487, 1650, 3074, 3132, 3180, 3254
syn-$CH_3COCHCl$	20, 1445, 213, 367, 502, 592, 629, 835, 945, 1010, 1042, 1207, 1376, 1414, 1482, 1490, 1678, 3068, 3127, 3175, 3239
anti-$CH_2ClCOCH_2$	40, 237, 389, 418, 498, 500, 773, 805, 857, 930, 1024, 1208, 1301, 1313, 1463, 1479, 1574, 3129, 3186, 3191, 3308
syn-$CH_2ClCOCH_2$	50, 216, 360, 366, 491, 576, 753, 779, 877, 929, 1015, 1199, 1204, 1353, 1465, 1477, 1648, 3102, 3151, 3173, 3289